MEAN TOPOLOGICAL EVOLUTION IN A TURBULENT BOUNDARY LAYER

Callum Atkinson, Julio Soria
Laboratory for Turbulence Research in Aerospace and Combustion
Department of Mechanical and Aerospace Engineering
Monash University
Clayton, Victoria, 3800, Australia
cal.atkinson@gmail.com, julio.soria@monash.edu

Sergei Chumakov, Ivan Bermejo-Moreno
Center for Turbulence Research
Stanford University
California, 94305-3030, USA.
schumakov@gmail.com, ibermejo@stanford.edu

ABSTRACT

Lagrangian mean evolution of a developing zero pressure gradient turbulent boundary layer ($\mathrm{Re}_\theta = 730$ to 1954) is investigated using data from a direct numerical simulation performed by Wu & Moin (2010). Conditional mean trajectories (CMTs) for the evolution of the invariants of the velocity gradient tensor (VGT) are calculated based on the mean rate of change of the invariants, conditioned on their location in the (R_A, Q_A) invariants plane. Following Chong *et al.* (1990) the location in this plane distinguish the focal or non-focal nature of flow at that point, such that CMTs represent the mean topological evolution of points in the flow. In the present case CMTs for strong gradients in all regions of the boundary layer pass around a focus at the origin and asymptote towards the right-hand side of a saddle point located near the of the line dividing unstable focal and unstable nodal structures. Closer to the origin weaker gradients follow an almost periodic clockwise spiralling evolution from stable-focus stretching to unstable-focus contraction, unstable-node saddle/saddle and stable-node saddle/saddle topology. Increasing time-scales are observed for both the strong and weak gradient trajectories further above the wall. Mean time-scales associated with the spiralling evolution in terms of inner scales are 67.9 ν/u_τ^2 in the viscous layer, 151 ν/u_τ^2 in the buffer layer and 658 ν/u_τ^2 in the log and wake region or 1.25 estimated eddy turnover times.

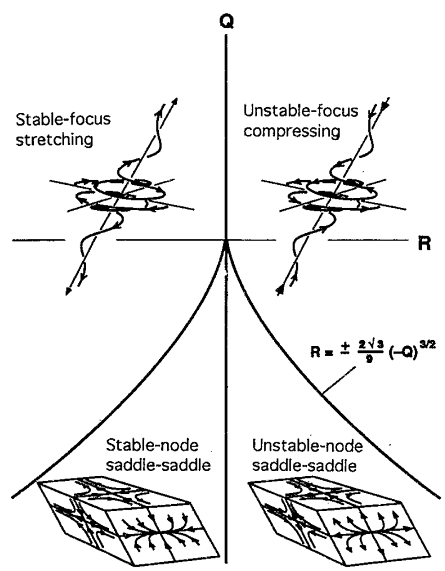

Figure 1. Three-dimensional local topologies in the (R_A, Q_A)-plane for incompressible flow. Taken from Soria *et al.* (1994).

INTRODUCTION

Reliable modelling or control of wall-bounded turbulent flows requires an understanding of the mechanisms behind the evolution and distribution of turbulence near the wall. Studies involving the temporal evolution of turbulent flows is complicated by the motion of each fluid particle and the dependence of many fluid properties on the relative motion of the observer. This is particularly true for wall-bounded flows which involve significant changes in convection velocity. Such analysis can be simplified by examining quantities such as the velocity gradient tensor (VGT) which is Galilean invariant and independent of a non-accelerating observer, and can be directly related to quantities such as enstrophy density and dissipation.

Following the topological approach introduced by

Chong, Perry & Cantwell (1990) the invariants of the VGT can be used to classify the local topology of any point in the flow (see figure 1), within a basis of critical point theory. This approach was first applied to the study of turbulent flow by Chen *et al.* (1990), where correlations were observed between the 2nd and 3rd invariants (Q_A and R_A) of the VGT in compressible and incompressible mixing layers. This behavior has since been observed in time-developing mixing layers by Soria *et al.* (1994), in turbulent channel flows by Blackburn *et al.* (1996), in turbulent boundary layers by Chacin *et al.* (1996) and in homogeneous isotropic turbulence by Martin *et al.* (1998), suggesting that many of these correlations and geometric flow features are common to all turbulent flows.

Martin *et al.* (1998) and Ooi *et al.* (1999) examined the evolution of flow topology using data from direct numerical simulations (DNS) of homogeneous isotropic turbulence, involving the conditional averaging of the time rate of change of the (R_A, Q_A) invariants and determination of conditional mean trajectories (CMTs) in the (R_A, Q_A)-plane. Points in the flow were observed to follow a clockwise spiral in this plane with a stable focus at the origin, indicating a cyclic topological change through unstable-node/saddle/saddle (UN/S/S), stable-node/saddle/saddle (SN/S/S), stable-focus/stretching (SF/S) to unstable-focus/contracting (UF/C). This cyclic was approximately periodic, with a characteristic period of 3 τ_{eddy}, where τ_{eddy} is the eddy turnover time.

CMTs for a turbulent boundary were examined by Chacin & Cantwell (2000) using the DNS of Spalart (1988) at $\mathrm{Re}_\theta = 300$. For most regions of the boundary layer particles were observed to move towards the origin $(R_A, Q_A) = (0,0)$ following asymptotes in the upper left and lower right quadrants, without the spiraling pattern that was observed in homogeneous isotropic turbulence. The only exception to this was in the viscous sublayer $y^+ < 5.6$, however this spiraling did not show asymptotic behavior. Using experimental tomographic particle image velocimetry data in a region $88 < y^+ < 240$ wall units Elsinga & Marusic (2010) calculated CMTs for a turbulent boundary layer at $\mathrm{Re}_\theta = 2460$, where a spiralling similar to that of homogeneous isotropic turbulence was observed. In this case the period was 14.3 δ/U_e, 470 ν/u_τ^2 or 1 τ_{eddy} in terms of outer, inner and eddy time-scales, respectively.

In this paper we present an investigation of the Lagrangian mean evolution of the invariants of the VGT in different regions of a developing turbulent boundary layer from $730 < \mathrm{Re}_\theta < 1954$ using data from a DNS of a zero pressure gradient turbulent boundary layer by Wu & Moin (2010). From this the mean time-scales associated with the topological evolution of structures in different regions of a turbulent boundary layer are extracted.

THEORETICAL BACKGROUND

Comprehensive background and derivation of the topological methodology and the relationship between the invariants of the velocity gradient tensor and local flow topology can be found in Chong *et al.* (1990); Cantwell (1992); Soria *et al.* (1994) among others. A brief summary, definitions and aspects relating to the present flow are presented below, with further details of models given in Atkinson *et al.* (2011).

The VGT $A_{ij} = \partial u_i/\partial x_j$ at a point in the flow has the characteristic equation:

$$\lambda_i^3 + P_A \lambda_i^2 + Q_A \lambda_i + R_A = 0, \tag{1}$$

where λ_i are the eigenvalues of A_{ij} and P_A, Q_A and R_A are the first, second and third invariants. For incompressible flows $P_A = -A_{ii} = 0$, meaning the local flow topology can be expressed in terms of the invariants Q_A and R_A, as given by the following expressions:

$$Q_A = -\tfrac{1}{2} A_{ij} A_{ji}, \tag{2}$$

$$R_A = -\tfrac{1}{3} A_{ij} A_{jk} A_{ki}. \tag{3}$$

Figure 1 shows the two-dimensional representation of the (R_A, Q_A)-plane and the regions associated with the four possible non-degenerate local flow topologies (stable-focus/stretching (SF/S), unstable-focus/contracting (UF/C), stable-node/saddle/saddle (SN/S/S) and unstable-node/saddle/saddle (UN/S/S)) that can exist in an incompressible flow. The tent-like curve represents the boundary between non-focal, dissipative motions (below the line) and focal, vortical fluid motions (above the line) and corresponds to $D_A = 0$, where D_A is the discriminant of A_{ij}:

$$D_A = \tfrac{27}{4} R_A^2 + Q_A^3. \tag{4}$$

Following Cantwell (1992) the evolution equation for A_{ij} in a Lagrangian frame of reference centred on a fluid particle can be obtained by differentiating the incompressible Navier-Stokes equations with respect to x_j:

$$\frac{\mathrm{D}A_{ij}}{\mathrm{D}t} + A_{ik}A_{kj} - (A_{km}A_{mk})\frac{\delta_{ij}}{3} = H_{ij}, \tag{5}$$

where $\mathrm{D}/\mathrm{D}t$ is the total derivative, δ_{ij} is the Kronecker delta and H_{ij} is a tensor consisting of the non local anisotropic pressure forces and the viscous diffusion, defined as,

$$H_{ij} = -\left(\frac{\partial^2 p}{\partial x_i \partial x_j} - \frac{\partial^2 p}{\partial x_k \partial x_k}\frac{\delta_{ij}}{3}\right) + \nu \frac{\partial^2 A_{ij}}{\partial x_k \partial x_k} \tag{6}$$

These equations represent a significant reduction in complexity when compare to the full Navier-Stokes equation, explaining the interest in Lagrangian flow models.

Evolution equations are derived from (5) in terms of the invariants Q_A, R_A and the tensor H_{ij} and given as:

$$\frac{\mathrm{D}Q_A}{\mathrm{D}t} = -3R_A - A_{ik}H_{ki}, \tag{7}$$

$$\frac{\mathrm{D}R_A}{\mathrm{D}t} = \tfrac{2}{3} Q_A^2 - A_{in}A_{nm}H_{mi}. \tag{8}$$

Similar evolution equations for Q_S, R_S, Q_W are presented by Ooi *et al.* (1999).

Region	y^+	*Datapoints* (nx, ny, nz)	$\langle Q_W \rangle_l \,/\, \langle Q_W \rangle_{\text{total}}$
Viscous layer	< 5	5520, 10, 256	69.4
Buffer layer	5 to 40	5520, 45, 256	12.6
Log and wake layer	40 to 1100	5520, 227, 256	0.28

Table 1. Turbulent boundary layer regions and the number of grid points in each region for a single snapshot of the DNS database.

DIRECT NUMERICAL SIMULATION DATABASE

The data used in this investigation was obtained from a DNS of an incompressible, ZPG flat plate boundary layer, performed by Wu & Moin (2010). Flow develops from a Blasius profile ($\mathrm{Re}_\theta = 80$) at the inlet and achieve a fully turbulent state at $\mathrm{Re}_\theta = 730$ and continues to grow to $\mathrm{Re}_\theta = 1950$. Transition was triggered by the periodic addition of patches of homogeneous isotropic turbulence to the freestream, controlled such that the streamwise pressure gradient remained negligible. Detail of the simulation grid and algorithm can be found in Wu & Moin (2009, 2010).

The present study was performed by considering the ensemble of the VGT and pressure Hessian at points in the fully turbulent zone from $\mathrm{Re}_\theta = 730$ to 1954. Three regions of throughout the boundary layer were examined as indicated in table 1. The height above the wall of each region was determined based on the mean skin friction and friction velocity over the fully turbulent domain. Over the length of the turbulent region the change in skin friction correspond to a change in height about the mean of ± 1, 3, and 5 grid point for the viscous, buffer and log layers, respectively. Six instantaneous statistically independent snapshots were considered. The contribution of each point to the statistics of that region, is weighted by the cell volume in order to remove bias associated with the concentration of points closer to the wall.

CONDITIONAL MEAN TRAJECTORIES

The mean temporal rate of change of the velocity gradient invariants can be determined by ensemble averaging the rate of change of the invariants, conditional on their location in the (R_A, Q_A)-plane. The rates of change of the invariants were evaluated using (7) and (8), based on the instantaneous VGT and pressure Hessian from the 6 DNS snapshots, at each point in the flow. To condition the averages of $\mathrm{D}Q/\mathrm{D}t$ and $\mathrm{D}R/\mathrm{D}t$ on the values of the invariant pair (R, Q), being invariants of the A_{ij}, S_{ij} or W_{ij}, the (R, Q)-plane is first divided into N_R, N_Q bins in the R and Q directions, such that there are an even number of bins in each direction over the region of interest. Following Ooi *et al.* (1999) the mean rate of change of the invariants in each bin is computed using the following discrete formulae:

$$\left\langle \frac{\mathrm{D}R}{\mathrm{D}t}\bigg|(R = R_0, Q = Q_0) \right\rangle = \frac{1}{N} \sum_{R_0-\Delta_R/2}^{R_0+\Delta_R/2} \sum_{Q_0-\Delta_Q/2}^{Q_0+\Delta_Q/2} \frac{\mathrm{D}R}{\mathrm{D}t}(R, Q), \quad (9)$$

$$\left\langle \frac{\mathrm{D}Q}{\mathrm{D}t}\bigg|(R = R_0, Q = Q_0) \right\rangle = \frac{1}{N} \sum_{R_0-\Delta_R/2}^{R_0+\Delta_R/2} \sum_{Q_0-\Delta_Q/2}^{Q_0+\Delta_Q/2} \frac{\mathrm{D}Q}{\mathrm{D}t}(R, Q), \quad (10)$$

where Δ_R and Δ_Q are the discrete bin widths in Q and R variable, and N is the number of samples in the bin spanning $R_0 - \Delta_R/2 < R < R_0 + \Delta_R/2$ and $Q_0 - \Delta_Q/2 < Q < Q_0 + \Delta_Q/2$. The result is the conditional rates of change for both variables at each point in the plane, representing a conditional mean vector field $(\mathrm{D}R/\mathrm{D}t(R, Q), \mathrm{D}Q/\mathrm{D}t(R, Q))$. This vector field is then used to calculate CMTs, representing the mean path followed by a point in the (R, Q)-plane as it evolves in time.

Resolution of the mean conditional vector fields and CMTs depend on the bin size. Smaller bin sizes increasing the resolution but do so at the expenses of the number of samples in the bin, as a finite number of points in the flow are distributed across an increasing number of bins. This can lead to wild fluctuations in the CMTs if statistical convergence is not achieved. In the viscous layer statistical convergence is achieved at $(0.005, 0.02)$ in the normalised (R_A, Q_A)-plane, located near the spiralling region of interest in the viscous layer, after approximately 7000 samples per bin, with convergence after 3000 per bin in the buffer layer at $(0.005, 0.02)$ and 20000 samples in log layers at (0.02,1.0). The effect of bin size on the mean conditional rate of change and the CMTs was investigated as detailed in Atkinson *et al.* (2011).

RESULTS AND DISCUSSION

Figures 2 shows the two-dimensional JPDFs of the invariants of the full velocity gradient tensor in (R_A, Q_A)-space for the viscous, buffer and log layer and wake regions. In each case the invariants have been normalised in terms $\langle Q_W \rangle_l$, representing the local mean value of Q_W in that region. JPDFs indicate that the boundary layer consist of mostly small gradients located at the origin, with contour levels typically possessing a self-similar shape, which indicates a tendency for points in the flow to be clustered around the $D_A = 0$ line and have mostly a SF/S or UN/S/S topology. As in channel flow at $\mathrm{Re}_\tau = 395$ (Blackburn *et al.*, 1996) and ZPG turbulent boundary layer at $\mathrm{Re}_\theta = 670$ (Chong *et al.*, 1998) the tear drop becomes more closely orientated with the right-hand side of the $D_A = 0$ line further from the wall and approaches the topology of homogeneous isotropic turbulence. Further from the wall points are distributed over a large portion of the (R_A, Q_A)-plane relative to the local mean Q_W, which is proportional to the local mean enstrophy. In terms of the total mean Q_W in the boundary layer (see table 1), the distribution is widest in the buffer layer indicating the largest range of scales, decreas-

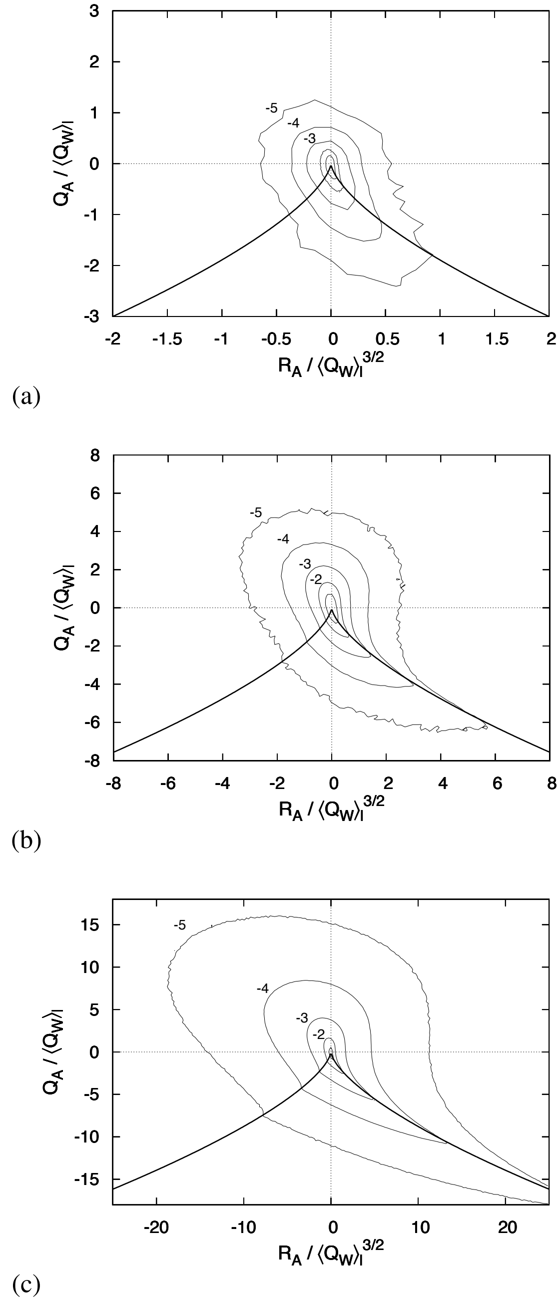

Figure 2. JPDF of the invariants R_A vs. Q_A for: (*a*) viscous layer; (*b*) buffer layer and (*c*) log and wake layers of a turbulent boundary layer from $\mathrm{Re}_\theta = 730$ to 1954. The difference between each contour line is one decade, with the exponents of the decade lines indicated. The tent like line represents the zero discriminant lines D_A for the VGT and strain rate tensor, respectively.

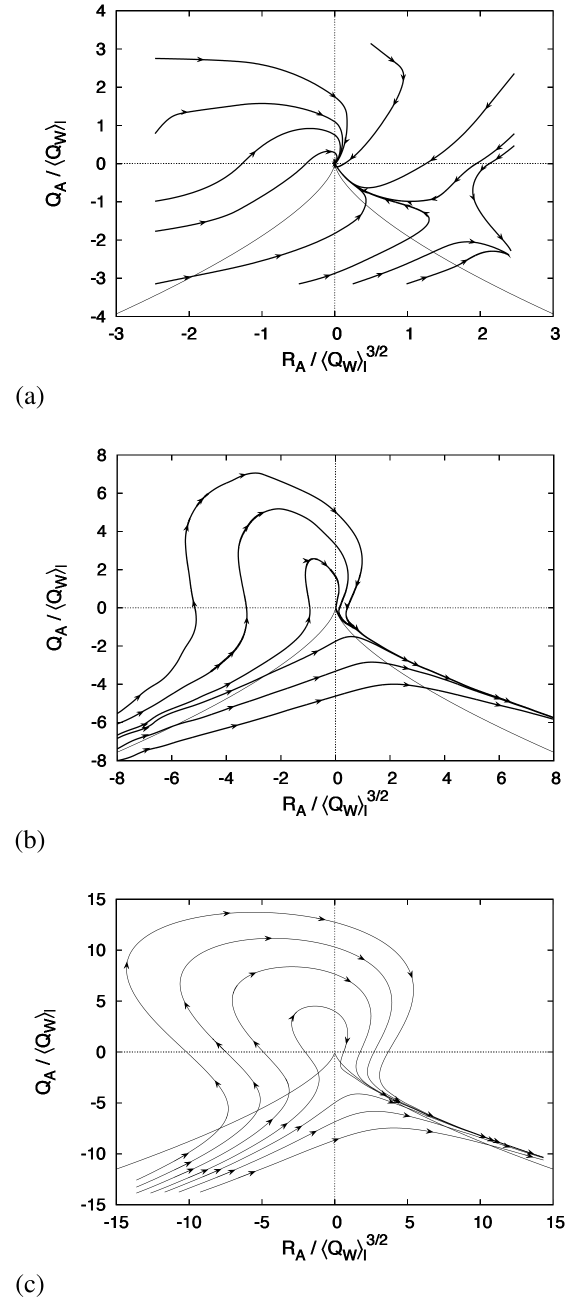

Figure 3. CMT in the (R_A, Q_A)-plane over a domain spanning approximately 5 decades of the JPDFs for: (*a*) viscous layer; (*b*) buffer layer and (*c*) log and wake layers of a turbulent boundary layer from $\mathrm{Re}_\theta = 730$ to 1954. The tent like line represents the zero discriminant lines D_A for the VGT.

ing significantly in the log and wake regions where only the gradients are present.

Figure 3 shows CMTs for the different regions of the boundary layer in the (R_A, Q_A)-plane, over domains corresponding to the 5 decades of the JPDFs of (R_A, Q_A). CMTs for the viscous layer show an attraction towards smaller gradients at the origin with a similar node and saddle point arrangement to those of the LMSE model (Dopazo *et al.*, 1993), where the viscous diffusion term in equation 6 is modelled using a linear mean square estimation and the pressure Hessian contribution is assumed to be negligible. This suggests that the LMSE model might be a reasonable model for large gradients, or small scale structures near the wall.

Further from the wall where the local mean enstrophy

$\langle Q_W \rangle_l$ has significantly decreased, CMTs for the buffer and log layers show trajectories separating from a line on the left-hand side and converging on the right-hand side. This is similar to the LMSE model with a larger time-scale and is consistent with a smaller relative contribution from the viscous diffusion term in (6) or increasing pressure Hessian terms. Unlike the LMSE model trajectories are not attracted to the $D_A = 0$ line exactly. In the buffer layer points separate and converge slightly the above $D_A = 0$ line, suggesting a mean evolution from SF/S to UF/C, either directly or via a transition from SF/S, SN/S/S, UN/S/S to UF/C. In the log and wake regions this divergence on the left-hand side occurs below $D_A = 0$ and converges slightly above, suggesting a mean evolution from SN/S/S to UF/C.

In the viscous layer the evolution of most points directly towards the origin, or in the buffer and log layer to remain remain focal or non-focal, is associated with the larger gradients, which the JPDF shows to represent only a small percentage of the flow. Most of the flow is clustered much closer to the origin of the (R_A, Q_A)-plane and as shown in figure 4 follows a spiralling pattern, similar to that observed in homogeneous isotropic turbulence by Martin *et al.* (1998). This involves a clockwise cycle that appears to originate at a saddle point corresponding to a local UN/S/S flow topology then undergoes a transition to SN/S/S, SF/S, UF/C. The spiral appears to have a focus slightly above the origin in the SF/S zone. This behaviour is not captured by the LMSE and is therefore thought to be associated with terms in the pressure Hessian.

CMTs produced by Elsinga & Marusic (2010) for a turbulent boundary layer at $\mathrm{Re}_\theta = 2460$ show a similar clockwise spiralling centred around the origin for a region $88 < y^+ < 240$ largely situated in the log layer. The shape of this spiral is similar to that observed in the log and wake region in the current simulation, yet show no signs of the asymptotes observed in the present simulation at larger gradients. This is likely the result of the measurement noise, and spatial filtering that is typically involved in experimental tomographic PIV measurements (Atkinson *et al.*, 2010), which filters out the strong local flow gradients and small-scale structures.

The mean evolution time-scales for each region of the turbulent boundary layer are presented in table 2 in terms of the inner and outer units and the eddy turnover time, estimated as $\tau_{eddy} = \delta / u_{rms}$ where u_{rms} is taken from the middle of the boundary layer. Time-scales increase with height above the wall, which could be related to increasing eddy sizes and an increasing turbulent length scale away from the wall. In the log and wake region the time-scale corresponds to 1.25 δ / u_{rms} or 1.25 τ_{eddy}, which is slight larger than the 1 τ_{eddy} observed by Elsinga & Marusic (2010) in the log layer alone. The longer time-scale in the present investigation maybe associated with the inclusion of the wake layer, where the time-scale is expected to be closer to 3 τ_{eddy} observed by Martin *et al.* (1998) in homogeneous isotropic turbulence.

Variation in the time-scale and the percentage of the cycle spent in each region of the (R_A, Q_A)-plane are examined further in Atkinson *et al.* (2011).

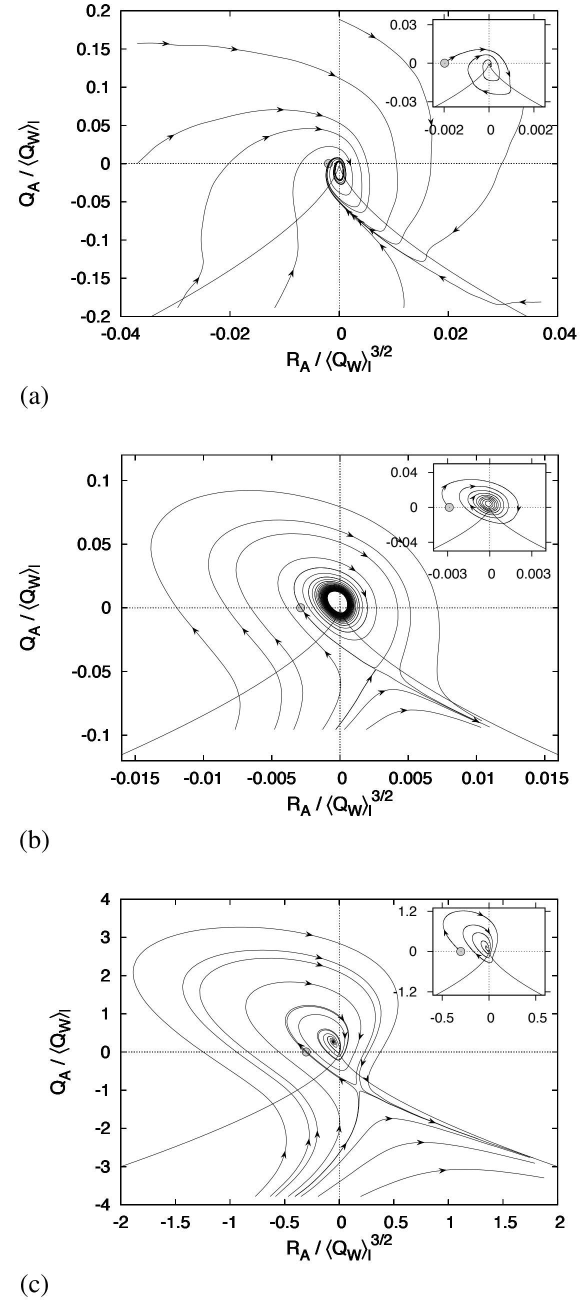

Figure 4. CMT in the (R_A, Q_A)-plane near the origin for: (*a*) viscous layer; (*b*) buffer layer and (*c*) log and wake layers of a turbulent boundary layer from $\mathrm{Re}_\theta = 730$ to 1954. The tent like line represents the zero discriminant lines D_A for the VGT. Inserts show the spiral pattern around the origin.

CONCLUSIONS

Lagrangian evolution of points in the viscous layer, buffer layer and log and wake layer of a turbulent boundary layer at $\mathrm{Re}_\theta = 730$ to 1954 are investigated in terms of invariants of the VGT and the conditional mean evolution trajectories in the (R_A, Q_A)-plane. CMTs for strong gradients (large values of (R_A, Q_A)) show a separation from the left-hand side of the boundary between focal and non-focal structures and an

Region	$t/\langle Q_W \rangle_l^{1/2}$	$t/(\nu/u_\tau^2)$	$t/(\delta/U_e)$	$t/(\delta/u_{rms})$
Viscous layer	36.5	67.9	2.10	0.130
Buffer layer	34.5	151	4.65	0.288
Log and wake layer	22.4	658	20.3	1.26

Table 2. Mean evolution time-scales associated with spiralling CMTs in each region of the boundary layer, where $\langle Q_W \rangle_l^{1/2}$ is proportional to the mean local enstrophy in that region of the boundary layer, ν/u_τ^2 is the inner time-scale, δ/U_e is the outer unit time-scale and δ/u_{rms} is the estimated eddy-turnover time.

attraction to the right-hand side with a focus at the origin and a saddle near the right-hand side, similar to the LMSE model for the evolution of the VGT when the anisotropic terms in the pressure Hessian are negligible. As the height above the wall increases comparisons with the LMSE model suggest a weaker contribution form the viscous diffusion terms in the VGT evolution equation.

CMTs change significantly near the origin of the (R_A, Q_A)-plane, where an almost periodic clockwise spiralling evolution from SF/S to UF/C, UN/S/S, SN/SS is observed for these weaker gradients at all stations through the boundary layer. The shape of the trajectories changes with height above the wall, transitioning from a largely oval trajectory where most of the time is spent with focal topology, to a more tear drop trajectory where the majority of time is spent as UN/S/S. Similar CMTs are observed for lower resolution log layer data by Elsinga & Marusic (2010), suggesting that this spiralling evolution represents the mean life-cycle of large scale structures in the flow. The mean time-scales associated with this evolution are 67.9 ν/u_τ^2 in the viscous layer, 151 ν/u_τ^2 in the buffer layer and 658 ν/u_τ^2 in the log and wake region or 1.25 estimated eddy turnover times.

ACKNOWLEDGEMENTS

The authors would like to thank Associate Professor Xiaohua Wu for graciously providing the DNS data that was used in this study. This research was instigated as part of a Center for Turbulence Research (CTR) Summer Program grant and was supported by a grant from the Australian Research Council, both of which are gratefully acknowledged. C.A. was supported by an Australian Postgraduate Award while undertaking this investigation.

REFERENCES

Atkinson, C., Chumakov, S., Bermejo-Moreno, I. & Soria, J. 2011 Topological evolution of a turbulent boundary layer. *J. Fluid Mech.* **submitted**.

Atkinson, Callum, Coudert, Sebastien, Foucaut, Jean-Marc, Stanislas, Michel & Soria, Julio 2010 The accuracy of tomographic particle image velocimetry for measurements of a turbulent boundary layer. *Experiments in Fluids* pp. 1–26, 10.1007/s00348-010-1004-z.

Blackburn, H. M., Mansour, N. N. & Cantwell, B. J. 1996 Topology of fine-scale motions in turbulent channel flow. *J. Fluid Mech.* **310**, 269–292.

Cantwell, B. J. 1992 Exact solution of a restricted euler equation for the velocity gradient tensor. *Phys. Fluids A* **4**, 782–793.

Chacin, J. M. & Cantwell, B. J. 2000 Dynamics of a low Reynolds number turbulent boundary layer. *J. Fluid Mech.* **404**, 87–115.

Chacin, J. M., Cantwell, B. J. & Kline, S. J. 1996 Study of turbulent boundary layer structure using the invariants of the velocity gradient tensor. *Exp. ThermL Fluid Sci.* **13**, 308–317.

Chen, J., Wong, M. S., Soria, J., Sondergaard, R., Perry, A. E., Rogers, M., Moser, R. & Cantwell, B. J. 1990 A study of the topology of dissipating motions in direct numerical simulations of time-developing compressible and in-compressible mixing layers. In *Proc. Summer Program 1990*. Center for Turbulence Research, Stanford University.

Chong, M.S., Soria, J., Perry, A.E., Chacin, J., Cantwell, B.J. & NA, Y. 1998 Turbulence structures of wall-bounded shear flows found using dns data. *J. Fluid Mech.* **357**, 225–247.

Chong, M. S., Perry, A. E. & Cantwell, B. J. 1990 A general classification of three-dimensional flow fields. *Phys. Fluids* **2** (5), 765–777.

Dopazo, C., no, L. Vali & Martin, J. 1993 Velocity gradients in turbulent flows. stochastic models. In *Ninth Symposium on Turbulent Shear Flows*. Kyoto, Japan.

Elsinga, G. E. & Marusic, I. 2010 Evolution and lifetimes of flow topology in a turbulent boundary layer. *Phys. Fluids* **22**.

Martin, J., Ooi, A., Chong, M. S. & Soria, J. 1998 Dynamics of the velocity gradient tensor invariants in isotropic turbulence. *Phys. Fluids* **10**, 2336–2346.

Ooi, A., Martin, J., Soria, J. & Chong, M. S. 1999 A study of the evolution and characteristics of the invariants of the velocity-gradient tensor in isotropic turbulence. *J. Fluid Mech.* **381**, 141–174.

Soria, J., Sondergaard, R., Cantwell, B. J., Chong, M. S. & Perry, A. E. 1994 A study of the fine-scale motions of incompressible time-developing mixing layers. *Phys. Fluids* **6**, 871–884.

Spalart, P. R. 1988 Direct simulation of a turbulent boundary layer up to re$_\theta$ = 1410. *J. Fluid Mech.* **187**, 61–98.

Wu, X. & Moin, P. 2009 Direct numerical simulation of turbulence in a nominally zero-pressure-gradient flat-plate boundary layer. *J. Fluid Mech.* **630**, 5–41.

Wu, X. & Moin, P. 2010 Transitional and turbulent boundary layer with heat transfer. *Phys. Fluids* **22**.